# In vivo evaluation of a pro-healing polydopamine coated stent through an in-stent restenosis rat model

Adrien Hertault, Feng Chai, Mickael Maton, Jonathan Sobocinski, Patrice Woisel, Blandine Maurel, Joël Lyskawa, Nicolas Blanchemain

# In-vivo evaluation of a pro-healing polydopamine coated stent through in-stent restenosis rat model

Adrien Hertault [a,b], Feng Chai [a], Mickael Maton [a], Jonathan Sobocinski [a,c], Patrice Woisel [d], Blancdine Maurel [e], Joël Lyskawa [d] and Nicolas Blanchemain [a*]

Drug-eluting stents have demonstrated efficiency on in-stent restenosis (ISR) but induce a risk of late acute thrombosis by delaying strut re-endothelialization. Polydopamine (PDA), a biocompatible polymer inspired from adhesive proteins of mussels, has been reported to promote endothelial cells (EC) proliferation while limiting SMC proliferation in vitro, thus suggesting a pro-healing potential. This study aimed at evaluating in vivo the impact of the pro-healing PDA-coated stent on ISR and on the quality of the struts re-endothelialization in a rat model. PDA-coated stents demonstrated a significant reduction in ISR in vivo compared to bare metal stents (ratio neointima/media = 0.48 (+/- 0.26) versus 0.83 (+/- 0.42), p<0.001). Western blot analyses identified a trend towards an increased activation of p38 MAPK phosphorylation and its anti-proliferative effects on vascular SMC that could explain the results observed in morphological analyses. This bioinspired and biocompatible polydopamine layer could intrinsically limit ISR. In addition, according to its latent reactivity, PDA offers the possibility to immobilize some relevant drugs on PDA-functionalized stent to provide potential synergistic effects.

*a. Univ. Lille, INSERM, CHU Lille, U1008 - Controlled Drug Delivery Systems and Biomaterials, F-59000 Lille, France*
*b. Vascular & Endovascular Surgery Department, Valenciennes Hospital, France*
*c. Aortic Center, Heart & Lung Institute, Lille University Hospital, France*
*d. Univ. Lille, CNRS, INRAE, Centrale Lille, UMR 8207 - UMET - Unité Matériaux et Transformations, F-59000 Lille, France*
*e. INSERM, Université de Nantes, UMR1238, Phy-Os, Sarcomes osseux et remodelage des tissus calcifiés, F-44035 Nantes, France*

## 1. Introduction

Cardiovascular disease is a major health issue in western countries. Endovascular treatment, especially stent implantation, is a first-line option when symptoms arise in the coronaries or in the lower limb. However, bare metal stent (BMS) implantation is associated with a high rate (17 to 41% of the patients (1)) of in-stent restenosis (ISR) at mid-term and responsible for recurrence of symptoms and additional healthcare costs (2). ISR involves complex inter-related molecular and cellular mechanisms, which can be divided into an ‘‘early’’ (days to weeks) and a ‘‘late’’ (weeks to months) phases. Stent implantation induces a mechanical injury to the arterial wall with media dissection and endothelial disruption. The dysfunctional endothelium produces factors that promote thrombus formation, before fibrin and platelet aggregation provide the basis of a local systemic inflammatory response (3). During the late phase, vascular smooth muscle cells (VSMC), normally highly differentiated, change their phenotype, become hypertrophic and then proliferate and migrate at a high rate. This aberrant VSMC growth associated with coordinated extracellular matrix synthesis leads to neointima hyperplasia and ISR (4).

In order to decrease ISR, drug-eluting stents (DES) were designed to inhibit VSMC proliferation. The first-generation of DES focused on delivering anti-proliferative drugs e.g. paclitaxel or sirolimus, via non-resorbable polymers coating on the metallic surface. They have demonstrated efficiency on ISR but induce a high risk of late acute thrombosis due to a delayed strut re-endothelialization and a prolonged inflammatory response due to the non-resorbable character of the polymers (5,6). Dual antiplatelet therapy is required for patients to avoid acute thrombosis, but it is associated with a higher risk of hemorrhagic complications, potentially fatal. Virtually, the first-generation of DES did not demonstrate any improvements in terms of mortality at two years (7).

In order to improve the existing situation, three main axes of research have been defined to develop the next generations of DES. The first axis is to develop fully bioabsorbable stents, that would avoid prolonged injuries to the arterial wall and offer a complete recovery. Unfortunately, current results are disappointing with a lack of radial force, a high rate of stent fracture and thrombosis due to the inflammatory response (8). The second axis is to limit the use of pro-inflammatory polymers as drug carrier (biocompatible polymer including polymer free platform, resorbable and non-resorbable polymer). The third axis is to use a pro-healing drug (i.e. promoting re-endothelialization) rather than an antiproliferative drug that blindly limit cell proliferation. By early restoration of endothelial integrity, they may offer an alternative to provide a more effective long-term result of the revascularization. Interestingly, the second and third generation of DES based on biocompatible polymer coatings or polymer-free platforms have improved outcomes compared to the first-generation DES (9–12).

In this context, polydopamine (PDA), an adhesive polymer inspired from marine mussels, according to its strong adherence

properties and biocompatible features has sparkled great interest as a biomimetic coating for the functionalization of a wide range of materials including biomaterials such as stainless steel (316L SS), titanium and Cobalt-chromium (CoCr) (13).

Recently, significant efforts were devoted to understand the nature of polydopamine structure. It is generally well accepted that PDA coating formation involves the auto-oxidation of dopamine in quinone which rearranged to form 5,6-dihydroxyindole (DHI) (14). This monomer and unreacted free-dopamine/quinone molecule react to form covalent aryl-aryl linkages (15) leading to the formation of the polymeric structure of pDA containing a mixture of catechol, quinone, indole, and amine functional groups. Recently, it was reported that pDA chain growth occurs at the solid—liquid interface, where film formation likely starts with adsorption of small oligomeric species, which undergo further polymerization and maturation to form higher-molecular-weight pDA chains (16). Another hypothesis is that pDA is a supramolecular aggregate of monomeric and/or oligomeric species comprising a mixture of dopamine, dopamine-quinone, DHI or eumelanin-like derivatives that are held together through relatively weak interactions such as hydrogen bonding, charge transfer, π–π stacking, and π–cation assembly (17, 18). In particular, Ischia et al. claimed that this polydopamine film is composed of three building blocks containing 5,6-dihydroxyindole units, uncyclized catecholamine/quinone moieties and pyrrolecarboxylic acid fragments (19).

Recently, our group exploited this PDA adhesive layer to enable the grafting of (i) an anti-platelet adhesion and anti-thrombotic drug (20) and (ii) a polycyclodextrin-based drug delivery system onto CoCr vascular stents (21) and titanium surfaces respectively (22). In particular, PDA or multi-layered PDA coatings were employed in the context of vascular applications for the functionalization of 316L SS(23,24) or magnesium alloy(24) stent surfaces and it was established that the polydopamine layer improves endothelial cells proliferation while smooth muscle cells proliferation was inhibited in vitro (23,25), thus implying an intrinsic pro-healing effect on the vascular wall. Interestingly, in addition to their strong adherence properties such PDA films exhibit latent reactivity towards nucleophiles such as amines and thiols that can be further exploited to anchor various pro-healing biomolecules on the stent surface.

In this way, in-vivo studies have reported the pro-healing effect of various drugs coated via polydopamine layers (26–30) such as selenocystamine, Cu-MOFs (copper-based metal organic frameworks), Akt1-siRNA or VEGF in rat, dog or rabbit models. However, none have reported the in-vivo effect of polydopamine alone while its in-vitro pro-healing effect is well described.

It is therefore questionable whether the PDA alone would not already possess an interesting pro-healing effect in-vivo. The aim of this article is (i) to study in vitro the importance of the PDA and multi-layered PDA coatings on the cellular response and (ii) evaluate in vivo the pro-healing potential of PDA-coated stents through a rat model dedicated to ISR.

## 2. Materials and Methods

### 2.1. Materials and reagents

CoCr disks were cut from a cobalt−chromium rod (⌀ 14.5 mm) according to ISO standards 5832-12 (Co 66.00 %, Cr 27.34 %, Mo 5.19 %, Mn 0.56 %, Si 0.39 %) bought from Böhler-Edelstahl, Germany with a thickness of 3 mm each. CoCr disks were prepared and successively polished (4 cycles of 6 min each with 600, 1200, 2400 and supra5 sandpapers, PRESI, France) to obtain mirror-like surfaces. CoCr stents (Multi-link Mini Vision, 2.5 mm of diameter) were provided by Abbott Vascular® (Abbot Vascular, Santa Clara, USA). Each sample were pre-treated in an oxidative "Piranha" solution mixture with a 70/30 (v/v) ratio between sulfuric acid ($H_2SO_4$, 97 wt %, Fisher Scientific, Illkirch, France) and hydrogen peroxide ($H_2O_2$, 36 wt %, Sigma Aldrich, Saint Louis, USA) during 60 hours at room temperature under extractor hood. Samples were then rinsed four times in deionized water (18 MΩ, Veolia Waters Technologies, Saint Maurice, France) during 30 minutes under sonication and dried with nitrogen flow.

### 2.2. Functionalization of CoCr support

PDA coating was performed by dip coating according to our previously reported protocol (21) (defined later in the manuscript as our standard protocol): (i) CoCr supports (stents or disks) were immersed in 5 mL of dopamine solution (2 mg/mL) (Sigma Aldrich, Saint Louis, USA) in a 10mM Trizma buffer (Sigma Aldrich, Saint Louis, USA ) adjusted to pH 8.5. Reaction occurred during 12 hours at room temperature under 400 rpm. (ii) Samples were rinsed three times in deionized water under sonication (10 min) to eliminate poorly fixed dopamine. (iii) Samples were dried (37°C, overnight) before a thermal treatment of 1 hour at 150°C in a ventilated oven to obtain the PDA coating. Samples were referred as PDA-disks or PDA-stents.

Multi-layered PDA samples (labelled PDAm) were prepared by repeating successively three times each steps i) and ii) of the functionalization process. Samples were referred as PDAm-disks or PDAm-stents (23). Samples were finally sterilized by dipping in absolute ethanol during 5 min and stored at room temperature before being used.

### 2.3. Surface characterization

Surface morphology and thickness were investigated by Scanning Electron Microscopy (SEM) on a Hitachi S-4700 SEM field emission gun (FEG) operating with an acceleration voltage ranging from 3 to 6 KeV. A thin layer of carbon was previously sprayed onto the samples. The PDA-layer thickness was estimated with a scratch test.

### 2.4. In vitro biological evaluation

All experiments with blood were performed in accordance with the French regulation on Bioethics, and experiments were approved by the ethics committee at Lille university. Informed consents were obtained from human participants of this study

#### 2.4.1. Cell proliferation

The in vitro evaluations of PDA coating cytocompatibility were performed according to ISO 10993-5 with primary cultures of

Human Umbilic Vascular Endothelial Cells (HUVEC, Promocell, GmbH, Heidelberg, Germany) and Human Umbilic Arterial Smooth Muscle Cells (HUASMC, Promocell, GmbH, Heidelberg, Germany). HUVEC were cultured in Endothelial Cell Growth medium MV (Promocell GmbH, Heidelberg, Germany) enriched with Endothelial Cell Growth SupplementMix (Promocell, GmbH, Heidelberg, Germany) and gentamicin (40 µg/mL, Panpharma, Luitré, France). HUASMC were cultured in Smooth Muscle Cell Growth medium 2 (Promocell GmbH, Heidelberg, Germany) enriched with Smooth Muscle Cell Growth Supplement Mix (Promocell, GmbH, Heidelberg, Germany) and gentamicin (40 µg/mL). Cells were cultured at 37°C in a CO2 incubator (MCO-17AI, Sanyo, Osaka, Japan) with 5% CO2 and 100% relative humidity. All samples were sterilized in ethanol (96 %) for 1 min and drying under the laminar flow hood.

Disk samples (Ø 14.5 mm) were placed at the bottom of 24-wells cell culture plates (COSTAR®, Starlab, France) and 10 000 cells in 1 mL of culture medium were seeded in each well. The cell proliferation was assessed after 1 and 3 days using the non-toxic AlamarBlue dye (UptiBlueTM, Interchim, France), since an increase of Alamarblue® metabolism over time is often used as an indicator of cell proliferation. Briefly, the culture medium was removed and 500 µL of diluted Alamarblue dye were added to each sample. After 3 h incubation, 150 µL of this solution were transferred to a 96-well plate (Fluoro-LumiNuncTM, ThermoScientific, France) and the fluorescence was measured with a Twinkle LB970TM fluorometer (Berthold, France) at an excitation wavelength of 530 nm and at an emission wavelength of 590 nm. The data of fluorescence intensity are normalized and expressed as the mean percentage ± SD of three separate experiments with respect to the control (CoCr, 100%).

#### 2.4.2. Microscopic analysis of the actin cytoskeleton

The cells alignment and the focal adhesion contact to the substrate were observed after staining the actin filaments. All the chemical products applied in the following experiment were purchased from Sigma-Aldrich, UK. Briefly, as described in above-mentioned cell proliferation assay, the cells were fixed after 1 and 3 days of culture with 2% paraformaldehyde at room temperature, permeabilized in phosphate-buffered saline (PBS) - Triton X-100 buffer and then blocked with 1% bovine serum albumin (BSA) in PBS. For visualizing the cytoskeletal organization, actin filaments were labelled with 1.2 µg/mL fluorescein isothiocyanate (FITC) -phalloidin and nuclei were counterstained by DAPI (1 µg/mL). After washing in buffer, the specimens were embedded in PBS–glycerol–DABCO mounting medium and examined an inverted confocal laser scanning microscope LSM 710 (Carl Zeiss, Jena, Germany).

#### 2.4.3. Hemolysis assay

Blood samples were collected from freshly collected from healthy volunteers in sodium citrate (0.109M) Vacutainer® blood collection tube (BD, Le Pont-de-Claix CEDEX, France). Samples were pre-conditioned in 6 mL 0.9% (w/v) sodium chloride solution for 30 min at 37°C. Sodium chloride was used alone as negative control and 0.1% Na2CO3 as positive control. 60 µL of whole blood were added to the specimens and further incubate at 37°C for 60 minutes, under agitation at 80 rpm. Solutions were collected and then centrifuged (Centrifuge 5415 R, Eppendorf AG, Germany) for 10 min at 3250 rpm, at room temperature. Absorbance was measured at 540 nm using a microplate reader (Apollo LB911TM - Berthold, France) to determine the released hemoglobin of lysed red blood cells. The experimentation was conducted in triplicate.

Hemolysis rate was calculated as follows: R = (A–C1)/(C2–C1) × 100%, R: hemolysis ratio (%), A: absorbance of the sample (OD), C1: absorbance of the negative controls (OD), C2: absorbance of the positive control (OD).

#### 2.4.4. Platelet adhesion test

Human blood was sampled as previously described. Platelet rich plasma (PRP) was prepared by centrifuging (Allegra X12-R centrifuger, Beckman Coulter, Fullerton, CA) the blood at 300 g and 25°C for 5 min. 100 µL of fresh PRP was added onto each disk surface and incubated for 45 min at 37°C. Non-adherent platelets were removed by gently rinsing the sample twice with a 0.9% NaCl solution. The quantification of adherent platelet was determined by measuring lactate dehydrogenase (LDH) activity with a LDH kit (Roche life sciences, Meylan Cedex, France) according to the manufacturer's recommendations. The LDH standard curve was plotted to estimate the platelet number for optical density (at 490 nm) obtained from LDH assay.

### 2.5. In vivo evaluation

All animal experiments were performed in accordance with the Guide for the Care and Use of Laboratory Animals(25) and the regulations of the French Ministry of Agriculture, and were approved by local Institutional Animal Care and Use Committee (N° CEEA 212011). All surgical procedures were performed by a single operator.

#### 2.5.1. Stent implantation

Adult male Wistar rats (350-400 g, Janvier Labs, Le Genest-Saint-Isle, France) were purchased and fed with a normal diet during one week. On the day of implantation, rats were randomly separated into two groups (CoCr-Stent or PDA-stent) of 10 rats each. Rats were anesthetized with intraperitoneal injection of ketamine 130 mg/kg (Virbac, Carros, France) and xylazine 14 mg/kg (Dechra, Northwich, UK). Infra-renal aorta was exposed through a median laparotomy and a systemic heparinization (300 UI/kg) was performed prior to the aortic clamping (Figure 1a). Stents (Ø 2.5 mm × length 12 ± 4 mm, Abbott vascular) were introduced through a transverse aortotomy on balloon catheters (Figure 1b) and expanded at nominal pressure (8 atm) with an oversizing in diameter of 30% compared to the native aorta (Figure 1c). Stent lengths were evenly distributed between the groups.

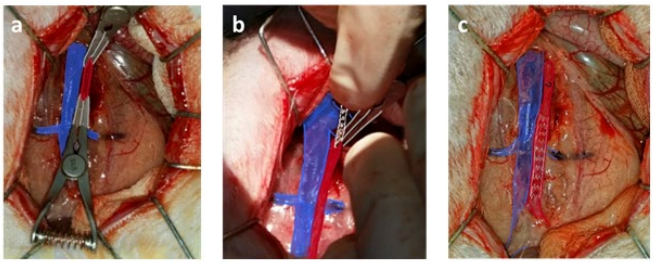


Figure 1: Aorta was accessed through a median laparotomy and clamped after general heparinization (injection in the inferior vena cava) (Figure 1a). Stent, mounted on balloon catheters, were introduced through a transversal aortotomy (Figure 1b), and deployed with an oversizing of 30% (Figure 1c).

At 7 or 28 days after stenting, the designated animals (described as follow) were anesthetized; after systemic heparinisation, the animals were sacrificed by intravenous injection of T61 (MSD, Courbevoie, France):

At day 7, among 4 animals of each group, stented arteries were isolated and frozen at -28°C for protein expression analysis; at day 28, for the 6 remaining animals of each group, stented arteries were perfused with fixative for histomorphometrical analysis purpose (5 rats) and electron microscopy analysis (TEM) (1 rat).

#### 2.5.2. Histomorphometrical analyses

Stented aortas were fixed in 4% paraformaldehyde phosphate-buffered solution, dehydrated, embedded in a polymethyl-methacrylate polymer (Technovit 9100 new, Heraeus, Germany) and stored one week at -20°C. 60-µm thick sections were cut along the embedded stented aortas. From each stented vessel, 15 to 25 sections were randomly chosen along the entire stented length, stained with hematoxylin/eosin (HE) and examined under a light microscopy (Leika DMIL, Ville, Germany) with magnification of ×10, digitized and recorded with a video camera (AxioCam ERc 5s, Carl Zeiss Microscopy, ville, Germany). The degree of in-stent stenosis was derived from the ratio of the measured area of neointima to that of the media (n/m ratio). Two-independent operators, who were blinded to the treatments, made the measurements with a computerized digital microscopic planimetry algorithm (ImageJ). The results were expressed as the average of all sections per stent ± standard deviation.

#### 2.5.3. Ultrastructure analyses by TEM

Stented aortas were fixed in 4% paraformaldehyde and 1% glutaraldehyde phosphate-buffer solution (pH 7.2) and then embedded in Epon resin (Epoxy embedding medium kit, Sigma Aldrich, Saint Louis, USA). Ultrathin sections (75 nm) were cut and contrasted with uranyl acetate and lead citrate before examination with a Jeon 1100 electron microscope (Tokyo, Japan) equipped with a Gatan digital camera driven by Digital Micropgraph software (Gatan, Pleasanton, USA). Those analyses allowed assessment of the quality of the reendothelialization of the struts of the stent.

#### 2.5.4. Western-blot analyses

Early-stage protein expression was determined by Western blot analyses on the frozen stented rat aorta at 7 days after stent deployment corresponding to the peak of the inflammatory response in this animal model. The analyses investigated the activating pathways of the smooth muscular cells proliferation mediated by Phospho-Kinase AktSER and Phospho-Kinase AktSER; and the inhibiting pathway of the proliferation mediated by MAP-Kinase P38. The antibodies were purchased from Cell Signaling (Danvers, USA). Stented aortic segments were placed in lysis buffer, and the stent was carefully removed under optical control. The vascular tissues were homogenized and centrifugated (10,000 g for 20 min at 4°C) to obtain the supernatant containing the proteins, which were quantified by Bradford method. 20 to 30 µg of protein were separated by a 10% sodium dodecyl sulfate-polyacrylamide electrophoresis gel, and then transferred to nitrocellulose membranes. Membranes were blocked with 5% nonfat dry milk followed by an incubation with anti-Phospho-Kinase AktSER antibody (1: 1000), anti-MAP-Kinase P38 antibody (1: 1000) or anti-MAP-Kinase P42/44 antibody (1: 1000) for 16 h at 4°C with gentle shaking. After being washed, membranes were incubated with secondary antibodies (horseradish peroxidase-conjugated anti-rabbit IgG, 1:2,000) for 1 h at 20°C. For chemiluminescent detection, membranes were treated with ECL reagent for 1 min and subsequently exposed to ECL hyperfilm (Western Lightning® Plus-ECL, PerkinElmer, France) for 1–2 min. The band density of the protein was quantified by densitometry using Multi Gauge V3.0 (FUJIFILM Graphic Systems France S.A.S., Bussy-Saint-Georges, France), and the results were expressed as a ratio of the active form (phosphorylated) to the total.

### 2.6. Statistical analysis

Quantitative variables were expressed as mean with standard deviation (SD) or median with interquartile range. Qualitative variables were presented with percentage and absolute number. Regarding continuous variables, comparison of two independent samples were performed with a Student t-test if normality was met, otherwise with a Mann-Whitney U test. Comparison of more than two samples were performed with a non-parametric Kolmogorov-Smirnov test. A p value $<0.05$ was considered as significant. All statistical analyses were performed with the SPSS software (IBM Corp. Released 2011. IBM SPSS Statistics for Windows, version 20.0. Armonk, NY: IBM Corp.).

## 3. Results

### 3.1. Sample morphologies

SEM analyses of coated CoCr surfaces revealed different morphologies between PDA and PDAm samples. Indeed, SEM images of the PDAm layer showed the presence of a large amount of aggregates on the CoCr surface. This layer appeared rougher compared to PDA that showed less but wider aggregates. In addition, the thickness of the PDAm layer estimated with a scratch made with a Teflon tip revealed a thicker coating (~200 nm) compared to PDA (~50 nm) (Figure 2). These results are in accordance with previous results dealing with PDA coating onto CoCr surfaces (21).

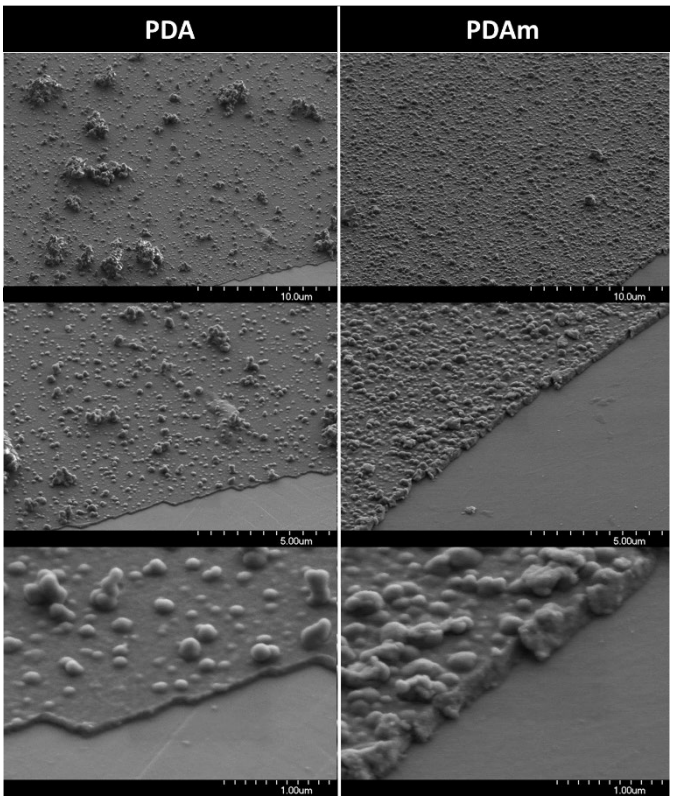


Figure 2: Representative SEM micrographs of PDA and PDAm samples.

### 3.2. In vitro experimentations

In vitro evaluation of cells growth (Figure 3a-b) and cell viability (Figure 3c-d) on the various coatings demonstrated at both 1 and 3 days, an increase of HUVEC vitality on PDA and PDAm coatings compared to bare chromium cobalt disks ($p<0.05$). No significant difference ($p>0.05$) was observed between PDAm and PDA coatings except on the first day where cell growth on PDA was slightly higher than that on PDAm. In contrast, at both 1 and 3 days (Figure 3c-d.), HUASMC vitality was significantly lower ($p<0.05$) for PDA and PDAm coatings compare to bare CoCr while no differences ($p>0.05$) were found between the two PDA coatings, except on the third day where cell growth on PDAm was lower than on PDA. Despite the above-mentioned differences between HUVEC and HUASMC, confocal microscopy (Figure 4) revealed that, on all tested substrates actin filaments were organized as a network of long and well-defined stress fibers typically spanning the entire cell body, which showed a good cytoskeleton function on the substrates.

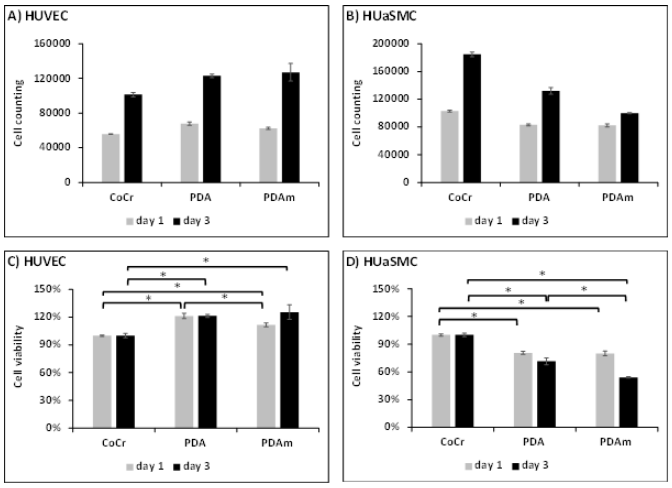


Figure 3: Cell counting of HUVEC (A) and HUASMC (B) and Cell viability of HUVEC (C) and HUASMC (B) after 1 day and 3 days of culture on PDA and PDAm sample (37 °C, 5% $CO_2$, 100% RH), without renewal of the culture medium (n=6). Significant difference between tested group and control (* $p < 0.05$)

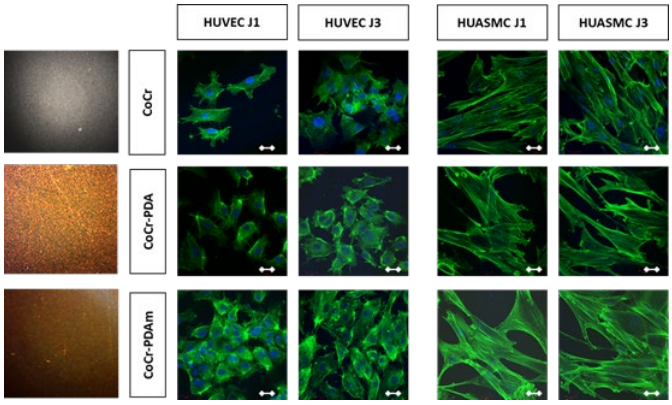


Figure 4: Actin staining with phalloin (green) show well-spreading cells on the different coatings on D1 and D3. Scale is represented on each picture as a white line with dots at each end and corresponds to 20µm.

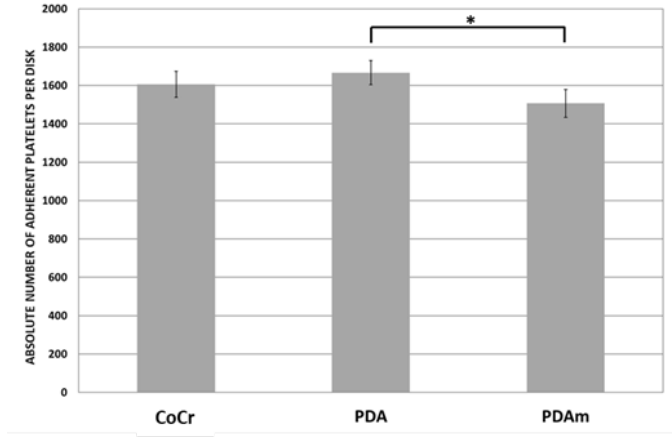


Figure 5: Platelet adhesion on PDA and PDAm surface (n=6). PRP was added on each disk surface during 45 min at 37°C. Significant difference between tested group and control (* $p < 0.05$)

Hemolysis tests showed the absence of hemolysis for all test samples. No differences between the negative control (NaCl) and the disk samples (CoCr, PDA and PDAm) was observed (Figure S1). Platelet adhesion rate (Figure 5) on CoCr samples was similar to those coated with PDA or PDAm but appeared slightly higher on PDA compare to PDAm ($p>0.05$).

As minor differences were observed in vitro between PDA and PDAm in accordance with previous results (21), in vivo experiments were conducted with the PDA layer to limit the number of animals required.

### 3.3. In vivo biological evaluation

Unfortunately, one rat in each group died during the post-operative course. Therefore, the following analyses on the stented rat aorta, at 28 days after stenting, were performed with 4 (instead of 5) rats per groups for histomorphological analyses: it revealed a significant reduction ($p<0.001$) in ISR after implantation of PDA stent (n/m = 0.48±0.26) compared to CoCr stent (n/m = 0.83±0.42) (Figure 6).

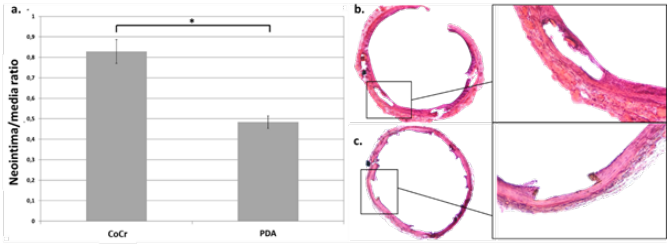


Figure 6: In-stent restenosis, estimated through the neointima/media (n/m) ratio was significantly lower on polydopamine (PDA) samples than on bare chromium-cobalt (CoCr) stent (a) (ratio n/m = 0.48 (+/- 0.26) versus 0.83 (+/- 0.42) respectively, $p<0.001$). Typical aspect of an aortic section 28th day after the stent implantation in the CoCr (b) and PDA (c) groups after eosin/hematoxillin coloration.

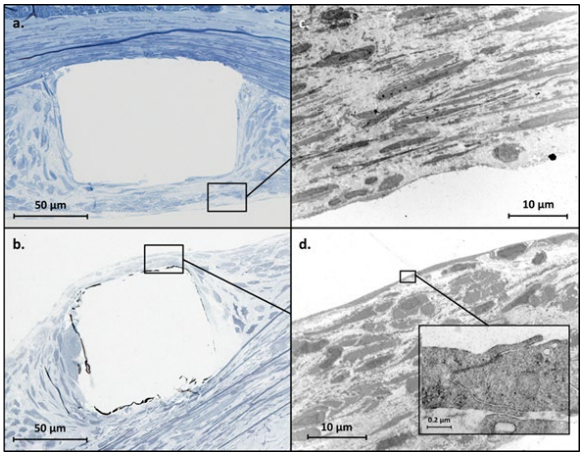


Figure 7: TEM analyses showed similar reendothelialization in the CoCr (a) and PDA (b) groups, suggesting there was no delay in the healing with the coating. Ultrastructures of the cells covering the struts seemed comparable in both groups (c,d), while the presence of a monolayer of cells with tight junctions in front of the lumen (d), compatible with endothelial cells is observed in the case of the PDA group.

TEM analyses revealed a thinner neointima covering (re-endothelialization) the stent struts in the PDA group (Figure 7b) compared with the CoCr group (Figure 7a) in agreement with our histologic analysis. The ultrastructure of the cells facing the arterial lumen was similar for both stents (Figure 7c-d).

On the western-blot analyses conducted on the 7th day after stenting, no differences were observed on the activating pathways of smooth muscular cells proliferation, since the activated form of Aktser (Figure 8a) and p42/44 (Figure 8b)) from PDA coated stents and bare CoCr stents were similar. However, the mediator of inhibiting pathway of vascular SMC proliferation, the MAPK P38, showed a trend towards higher activation rate on PDA stents than on CoCr (Figure 8c).

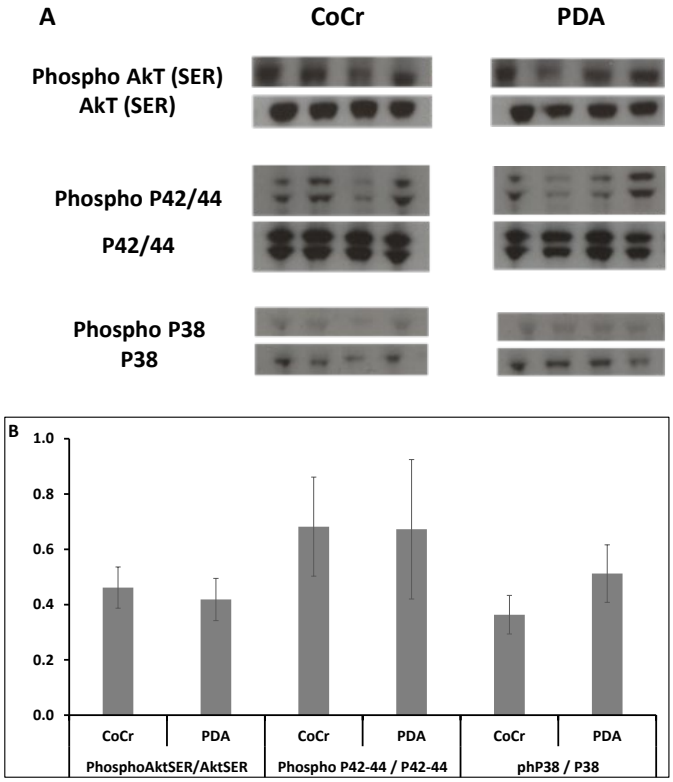


Figure 8: Western-blot analyses on day 7 after stent implantation of the activation pathways of smooth muscular cells proliferation, revealed no difference within the activated form of Aktser and p42/44, compared with their control (bare chromium-cobalt). However, analysis of the inhibition of the proliferation pathway mediated by p38 MAPK demonstrated a trend towards a higher rate of p38 MAPK phosphorylation, enhancing its anti-proliferative effects in vascular SMC which could explain the results observed in the histomorphometric analyses. No statistical differences were observed (Mann-Whitney U test).

## 4. Discussion

DES have been developed to overcome the major pitfall reported with vascular stents - restenosis. The first generation of DES (Cypher and Taxus) revolutionized interventional surgery but showed their limitations in terms of clinical results. Many strategies have been developed to improve outcomes with the second and third generation of stents. With regards to the coronary arteries, DES showed better results than BMS in terms of ISR. Indeed, the second generation of DES have partially overcome late acute stent thrombosis issues encountered with the first generation. However, the third generation, especially bioabsorbable scaffolds and polymer-free stents, have not demonstrated superiority to the gold standard of the second generation (a chromium-cobalt platform eluting everolimus via a durable polymer). This underscores the importance of further researches on pro-healing drug and/or polymeric scaffolds.

Yang et al. (23) and Zhong et al. (25) have reported an in vitro potential pro-healing effect of PDA layers, with selective inhibition of SMC and improvement of EC proliferation. In those studies, the PDA surfaces were obtained with three successive bathes of dopamine, with an intermediate step of sonication (deionized water), and a final drying step (one hour at 150°C). The surface coating obtained with their method are usually thicker and rougher than the ones obtained from our standard protocol consisting in one layer of PDA as observed with SEM (Figure 2) (21). Our hypothesis is that a single layer of PDA would be sufficient to observe an in-vitro and in-vivo pro-healing potential effect even the surfaces appeared different. Thus, in order confirm this hypothesis, we compared our standard protocol (PDA) to the protocol previously published by Yang et al. (23) (PDAm) and evaluating their respective impacts on in vitro biocompatibility.

As already demonstrated by Yang et al. (23), Hee Ku et al. (32) and Luo et al. (33), PDA coating was able to promote the EC proliferation. Nevertheless, no significant difference in terms of HUVEC proliferation at day 3 was observed between PDA and PDAm coating (fig. 3 a-b) suggesting that a monolayer was sufficient to improve EC proliferation as we hypothesized. In parallel, the inhibition on SMC proliferation was improved with both PDA and PDAm except on the third day where SMC cell growth on PDAm was a bit lower than on PDA (fig 3 c-d). These results could be attributed to different ratio of quinone/catechol groups exposed on the Co/Cr surfaces. Indeed, according to Ding et al. (34), modifications in the coating process (essentially in the initial dopamine solution concentration) would increase the ratio of quinone/catechol groups grafted onto the Co/Cr surface and, consequently the protein absorption rate (especially Fibronectin) resulting in EC proliferation by regulation of their adhesion. Moreover, the reactive catechol groups of polydopamine coating could be implicated in the SMC inhibition through their antioxidant properties. In the case of PDA sample, a thermal treatment at 150°C has shown to significantly increase the quinone proportion in the PDA layer (35) and consequently the protein absorption rate and subsequent endothelial cell proliferation. The observed differences between PDA and PDAm on surface roughness could also be implicated in the observed differences in cell populations' proliferation/inhibition or platelet adhesion. This possibility has not been specifically explored in this work.

Hemocompatibility is a major issue in the context of vascular devices. Yang et al. first demonstrated that platelet adhesion was significantly reduced on 316L steel samples coated with polydopamine (23) while Ding et al. reported a higher platelet adhesion rate on titanium surfaces coated with polydopamine (34), but they assumed that the strong binding properties of polydopamine for non-adhesive proteins such as serum albumin would lead to a surface passivation in vivo. In this publication, the authors suggested that even if the absorption of fibrinogen was higher on coated surfaces than on bare metal (which should induce higher adhesion rates), the absorbed fibrinogen on polydopamine was denatured and therefore lead to less platelet adhesion. In our study, PDAm coatings (similar to those used by Yang et al.) showed a trend towards a decreased platelet adhesion, but no significant difference was observed between CoCr and PDA samples.

As no major differences were observed between PDA and PDAm coatings in in vitro experimentations, in vivo studies were then conducted according to our standard PDA coating process to reduce animal assays. The neointima/media ratio was used as an indicator to estimate ISR. At day 28 post-stent implantation, the ISR was significantly lower with a stent functionalized by a polydopamine layer compare to bare stent (ratio n/m = 0.48 (+/- 0.26) versus 0.83 (+/- 0.42) respectively, $p<0.001$). Moreover, the TEM analysis, conducted to assess the quality of the reendothelialization of struts showed a thin layer of cells on the PDA-stent surface with a tight junction on the lumen side attributed to EC. Those results suggest that the pro-healing effect of polydopamine suspected in several in vitro studies would be maintained in vivo and could benefit to patients.

PDA-modified surfaces were reported to significantly enhance HUVEC adhesion, proliferation, and migration, release nitric oxide (NO)(23) and decrease the adhesion and proliferation of HUASMC. In this context, multiple cell signalling cascades control vascular SMC growth, including members of the MAPK family such as p42/44 and p38, as well as phosphatidylinositol 3-kinase (PI3K) and its downstream effector Akt. p42/44 seems to play a central role in the signalling cascade of proliferation (36). On the contrary, p38 MAPK seems to have anti-proliferative effects on vascular SMC (37). In our study, we reported in vivo a tendency to a higher rate of p38 MAPK activated form when PDA-stents are implanted, which might induce a protective effect against vascular SMC proliferation and restenosis.

In addition to this intrinsic pro-healing properties, polydopamine exhibit latent reactivity towards nucleophiles such amines and thiols which was exploited for the grafting of therapeutic agents or polymer (35,38,39) onto the stent surface to promote reendothelialization or to reduce ISR. These functions could be exploited for the further grafting of pro-healing drugs paving the way for promising perspectives in cardiovascular area.

## 5. Conclusion

This study confirms the in vitro pro-healing effect of the PDA coating layer through the reduction of smooth muscle cells proliferation and the improvement of the endothelial cells proliferation. Interestingly, this in vitro effect was maintained in vivo through a significant reduction of the restenosis after 28 days of implantation in a rat model thus demonstrating that this biocompatible PDA polymer could play a key role for the prevention of in-stent restenosis. This

anti-proliferative effect in vascular SMC might be explained by a higher rate of p38 MAPK phosphorylation. Interestingly, PDA has many reactive chemical functions in its structure (quinone, amines) that could be exploited to immobilize therapeutic molecules onto the stent surface. In this way, the grafting of an antiplatelet and / or antithrombotic molecule onto the stent surface represents a promising way to promote synergistic effects in the treatment of atherosclerotic lesions.

## 6. Suppl Data

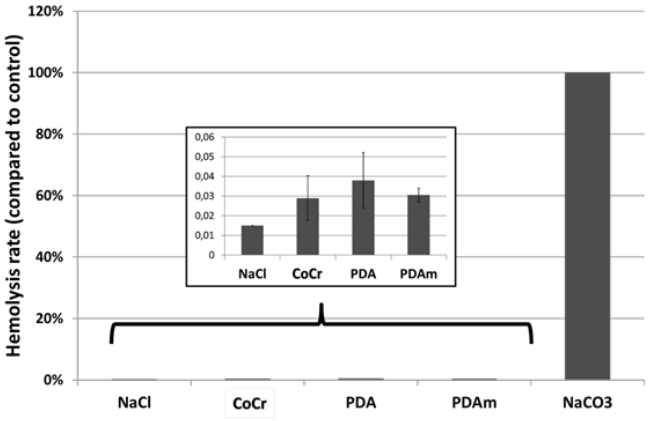


Figure S1: Hemolysis test showed no different hemolysis between the negative control (NaCl) and the different samples, when compared to full hemolysis of the sample (NaCO3).

## Conflicts of interest

There are no conflicts to declare.

## Acknowledgements

The authors would like to thank the Abbott Company for providing the vascular stents, and the French Society of Vascular Surgery (SCV) and INTERREG 2 Sea program (IMODE) for providing financial support to this project. The authors also thank the Plateforme Ressources Expérimentales, D.H.U.R.E, University of Lille, for their support on animal studies, Rustem UZEBOV and Ahmed ADDAD from Chevreul Institute for TEM and SEM analyses respectively.

## Notes and references

1 Buccheri D, Piraino D, Andolina G, Cortese B. Understanding and managing in-stent restenosis: a review of clinical data, from pathogenesis to treatment. J Thorac Dis. 2016 Oct;8(10):E1150–62.
2 Poder TG, Erraji J, Coulibaly LP, Koffi K. Percutaneous coronary intervention with second-generation drug-eluting stent versus bare-metal stent: Systematic review and cost–benefit analysis. PLOS ONE. 2017 mai;12(5):e0177476.
3 Mitra AK, Agrawal DK. In stent restenosis: bane of the stent era. J Clin Pathol. 2006 Mar;59(3):232–9.
4 Muto A, Fitzgerald TN, Pimiento JM, Maloney SP, Teso D, Paszkowiak JJ, et al. Smooth muscle cell signal transduction: implications of vascular biology for vascular surgeons. J Vasc Surg. 2007 Jun;45 Suppl A:A15-24.
5 Otsuka F, Nakano M, Ladich E, Kolodgie FD, Virmani R. Pathologic Etiologies of Late and Very Late Stent Thrombosis following First-Generation Drug-Eluting Stent Placement. Thrombosis. 2012;2012:608593.
6 van Beusekom HMM, Sorop O, van den Heuvel M, Onuma Y, Duncker DJ, Danser AHJ, et al. Endothelial function rather than endothelial restoration is altered in paclitaxel- as compared to bare metal-, sirolimusand tacrolimus-eluting stents. EuroIntervention J Eur Collab Work Group Interv Cardiol Eur Soc Cardiol. 2010 May;6(1):117–25.
7 Kastrati A, Mehilli J, Pache J, Kaiser C, Valgimigli M, Kelbaek H, et al. Analysis of 14 trials comparing sirolimus-eluting stents with bare-metal stents. N Engl J Med. 2007 Mar 8;356(10):1030–9.
8 Ali Ziad A., Gao Runlin, Kimura Takeshi, Onuma Yoshinobu, Kereiakes Dean J., Ellis Stephen G., et al. Three-Year Outcomes With the Absorb Bioresorbable Scaffold. Circulation. 2018 Jan 30;137(5):464–79.
9 Valgimigli M, Tebaldi M, Borghesi M, Vranckx P, Campo G, Tumscitz C, et al. Two-year outcomes after first- or second-generation drug-eluting or bare-metal stent implantation in all-comer patients undergoing percutaneous coronary intervention: a pre-specified analysis from the PRODIGY study (PROlonging Dual Antiplatelet Treatment After Grading stent-induced Intimal hyperplasia studY). JACC Cardiovasc Interv. 2014 Jan;7(1):20–8.
10 Smits PC, Vlachojannis GJ, McFadden EP, Royaards K-J, Wassing J, Joesoef KS, et al. Final 5-Year Follow-Up of a Randomized Controlled Trial of Everolimus- and Paclitaxel-Eluting Stents for Coronary Revascularization in Daily Practice: The COMPARE Trial (A Trial of Everolimus-Eluting Stents and Paclitaxel Stents for Coronary Revascularization in Daily Practice). JACC Cardiovasc Interv. 2015 Aug 17;8(9):1157–65.
11 Garot P, Morice M-C, Tresukosol D, Pocock SJ, Meredith IT, Abizaid A, et al. 2-Year Outcomes of High Bleeding Risk Patients After Polymer-Free Drug-Coated Stents. J Am Coll Cardiol. 2017 Jan 17;69(2):162–71.
12 Hofma SH, Brouwer J, Velders MA, van't Hof AWJ, Smits PC, Queré M, et al. Second-generation everolimus-eluting stents versus first-generation sirolimus-eluting stents in acute myocardial infarction. 1-year results of the randomized XAMI (XienceV Stent vs. Cypher Stent in Primary PCI for Acute Myocardial Infarction) trial. J Am Coll Cardiol. 2012 Jul 31;60(5):381–7.
13 Lee H, Dellatore SM, Miller WM, Messersmith PB. Mussel-Inspired Surface Chemistry for Multifunctional Coatings. Science. 2007 Oct 19;318(5849):426–30.
14 Liebscher J, Mrówczyński R, Scheidt HA, Filip C, Hădade ND, Turcu R et al. Structure of polydopamine: a never-ending story? Langmuir. 2013 Aug 20;29(33):10539-48.
15 D'Ischia M, Napolitano A, Pezzella A, Meredith P, Sarna T. Chemical and structural diversity in eumelanins: unexplored bio-optoelectronic materials. Angew Chem Int Ed Engl. 2009;48(22):3914-21
16 Delparastan P, Malollari KG, Lee H, Messersmith PB. Direct Evidence for the Polymeric Nature of Polydopamine. Angew Chem Int Ed Engl. 2019 Jan 21;58(4):1077-1082.
17 Hong S, Na YS, Choi S, Song IT, Kim WY, Lee H. Non-Covalent Self-Assembly and Covalent Polymerization Co-Contribute to Polydopamine Formation. Adv. Funct. Mater. 2012, 22, 4711-17
18 Hong S, Wang Y, Park SY, Lee H. Progressive fuzzy cation-π assembly of biological catecholamines. Science Advances 2018, 4, eaat7457.
19 Della Vecchia MF, Avolio R, Alfè M, Errico ME, Napolitano A, D'Ischia M. Building-Block Diversity in Polydopamine Underpins a Multifunctional Eumelanin-Type Platform

Tunable Through a Quinone Control Point. Adv. Funct. Mater. 2013, 23, 1331–1340
20 Bricout N, Chai F, Sobocinski J, Hertault A, Laure W, Ung A, et al. Immobilisation of an anti-platelet adhesion and anti-thrombotic drug (EP224283) on polydopamine coated vascular stent promoting anti-thrombogenic properties. Mater Sci Eng C. 2020 Aug 1;113:110967.
21 Sobocinski J, Laure W, Taha M, Courcot E, Chai F, Simon N, et al. Mussel inspired coating of a biocompatible cyclodextrin based polymer onto CoCr vascular stents. ACS Appl Mater Interfaces. 2014 Mar 12;6(5):3575–86.
22 Pérez-Anes A, Gargouri M, Laure W, Van Den Berghe H, Courcot E, Sobocinski J, et al. Bioinspired Titanium Drug Eluting Platforms Based on a Poly-β-cyclodextrin-Chitosan Layer-by-Layer Self-Assembly Targeting Infections. ACS Appl Mater Interfaces. 2015 Jun 17;7(23):12882–93.
23 Yang Z, Tu Q, Zhu Y, Luo R, Li X, Xie Y, et al. Mussel-inspired coating of polydopamine directs endothelial and smooth muscle cell fate for re-endothelialization of vascular devices. Adv Healthc Mater. 2012 Sep;1(5):548–59.
24 Xiaoli Liu ZZ, Xiaoli Liu ZZ. Multifunctional MgF2/Polydopamine Coating on Mg Alloy for Vascular Stent Application. J Mater Sci Technol. 2015 Jul 23;31(7):733–43.
25 Zhong S, Luo R, Wang X, Tang L, Wu J, Wang J, et al. Effects of polydopamine functionalized titanium dioxide nanotubes on endothelial cell and smooth muscle cell. Colloids Surf B Biointerfaces. 2014 Apr 1;116:553–60.
26 Weng Y, Song Q, Zhou Y, Zhang L, Wang J, Chen J, et al. Immobilization of selenocystamine on TiO2 surfaces for in situ catalytic generation of nitric oxide and potential application in intravascular stents. Biomaterials. 2011 Feb 1;32(5):1253–63.
27 Yang Z, Yang Y, Zhang L, Xiong K, Li X, Zhang F, et al. Mussel-inspired catalytic selenocystamine-dopamine coatings for long-term generation of therapeutic gas on cardiovascular stents. Biomaterials. 2018 Sep;178:1–10.
28 Che H-L, Bae I-H, Lim KS, Song IT, Lee H, Muthiah M, et al. Suppression of post-angioplasty restenosis with an Akt1 siRNA-embedded coronary stent in a rabbit model. Biomaterials. 2012 Nov;33(33):8548–56.
29 Fan Y, Zhang Y, Zhao Q, Xie Y, Luo R, Yang P, et al. Immobilization of nano Cu-MOFs with polydopamine coating for adaptable gasotransmitter generation and copper ion delivery on cardiovascular stents. Biomaterials. 2019 Jun;204:36–45.
30 Wang J, Li B, Li Z, Ren K, Jin L, Zhang S, et al. Electropolymerization of dopamine for surface modification of complex-shaped cardiovascular stents. Biomaterials. 2014 Sep 1;35(27):7679–89.
31 National Research Council (US) Committee for the Update of the Guide for the Care and Use of Laboratory Animals. Guide for the Care and Use of Laboratory Animals [Internet]. 8th ed. Washington (DC): National Academies Press (US); 2011. (The National Academies Collection: Reports funded by National Institutes of Health). Available from: http://www.ncbi.nlm.nih.gov/books/NBK54050/
32 Ku SH, Park CB. Human endothelial cell growth on mussel-inspired nanofiber scaffold for vascular tissue engineering. Biomaterials. 2010 Dec;31(36):9431–7.
33 Luo R, Tang L, Zhong S, Yang Z, Wang J, Weng Y, et al. In vitro investigation of enhanced hemocompatibility and endothelial cell proliferation associated with quinone-rich polydopamine coating. ACS Appl Mater Interfaces. 2013 Mar 13;5(5):1704–14.
34 Ding Y, Yang Z, Bi CWC, Yang M, Zhang J, Xu SL, et al. Modulation of protein adsorption, vascular cell selectivity and platelet adhesion by mussel-inspired surface functionalization. J Mater Chem B. 2014;2(24):3819–29.
35 Luo R, Tang L, Wang J, Zhao Y, Tu Q, Weng Y, et al. Improved immobilization of biomolecules to quinone-rich polydopamine for efficient surface functionalization. Colloids Surf B Biointerfaces. 2013 Jun 1;106:66–73.
36 Dzau VJ, Braun-Dullaeus RC, Sedding DG. Vascular proliferation and atherosclerosis: new perspectives and therapeutic strategies. Nat Med. 2002 Nov;8(11):1249–56.
37 Miura S-I, Matsuo Y, Kawamura A, Saku K. JTT-705 blocks cell proliferation and angiogenesis through p38 kinase/p27(kip1) and Ras/p21(waf1) pathways. Atherosclerosis. 2005 Oct;182(2):267–75.
38 Choi DH, Kang SN, Kim SM, Gobaa S, Park BJ, Kim IH, et al. Growth factors-loaded stents modified with hyaluronic acid and heparin for induction of rapid and tight re-endothelialization. Colloids Surf B Biointerfaces. 2016 May 1;141:602–10.
39 Chien C-Y, Tsai W-B. Poly(dopamine)-assisted immobilization of Arg-Gly-Asp peptides, hydroxyapatite, and bone morphogenic protein-2 on titanium to improve the osteogenesis of bone marrow stem cells. ACS Appl Mater Interfaces. 2013 Aug 14;5(15):6975–83.
40 Lowe HC, Schwartz RS, Mac Neill BD, Jang I-K, Hayase M, Rogers C, et al. The porcine coronary model of in-stent restenosis: current status in the era of drug-eluting stents. Catheter Cardiovasc Interv Off J Soc Card Angiogr Interv. 2003 Dec;60(4):515–23.